Amino Acids (2015) 47:2551–2560
DOI 10.1007/s00726-015-2046-6

ORIGINAL ARTICLE

Tyrosine- and tryptophan-coated gold nanoparticles inhibit amyloid aggregation of insulin

Kriti Dubey[1] · Bibin G. Anand[1] · Rahul Badhwar[1] · Ganesh Bagler[1] · P. N. Navya[2] · Hemant Kumar Daima[2] · Karunakar Kar[1]

Received: 2 April 2015 / Accepted: 7 July 2015 / Published online: 21 July 2015

Abstract Here, we have strategically synthesized stable gold ($AuNPs^{Tyr}$, $AuNPs^{Trp}$) and silver ($AgNPs^{Tyr}$) nanoparticles which are surface functionalized with either tyrosine or tryptophan residues and have examined their potential to inhibit amyloid aggregation of insulin. Inhibition of both spontaneous and seed-induced aggregation of insulin was observed in the presence of $AuNPs^{Tyr}$, $AgNPs^{Tyr}$, and $AuNPs^{Trp}$ nanoparticles. These nanoparticles also triggered the disassembly of insulin amyloid fibrils. Surface functionalization of amino acids appears to be important for the inhibition effect since isolated tryptophan and tyrosine molecules did not prevent insulin aggregation. Bioinformatics analysis predicts involvement of tyrosine in H-bonding interactions mediated by its C=O, $–NH_2$, and aromatic moiety. These results offer significant opportunities for developing nanoparticle-based therapeutics against diseases related to protein aggregation.

Handling Editor: H. S. Sharma.

Electronic supplementary material The online version of this article (doi:10.1007/s00726-015-2046-6) contains supplementary material, which is available to authorized users.

✉ Hemant Kumar Daima
hkdaima@gmail.com; hemant.daima@sit.ac.in

✉ Karunakar Kar
karunakarkar@gmail.com; kkar@iitj.ac.in

[1] Department of Biology, Indian Institute of Technology Jodhpur, Old Residency Road, Jodhpur, Rajasthan 342011, India

[2] Department of Biotechnology, Siddaganga Institute of Technology, Tumkur, Karnataka 572103, India

Keywords Amyloid aggregation · Tryptophan · Tyrosine · Insulin · Gold nanoparticles

Abbreviation

CD	Circular dichroism
$AuNPs^{Tyr}$	Tyrosine-coated gold nanoparticles
$AuNPs^{Trp}$	Tryptophan-coated gold nanoparticles
$AgNPs^{Tyr}$	Tyrosine-coated silver nanoparticles
T_m	Transition temperature

Introduction

Making of nanoparticles which are strategically surface coated or functionalized with potential drugs has become one of the most useful tools to target a number of medical complications. Aggregation of proteins into amyloid fibrils is a very important process in biology and a number of pathologies are known to be associated with amyloid aggregation of proteins (Aguzzi and O'Connor 2010; Greenwald and Riek 2010). So far ~35 different proteins are known to be associated with the onset of many neurodegenerative diseases (Greenwald and Riek 2010; Chiti and Dobson 2006). The process of protein aggregation is also a matter of much concern for the storage of protein therapeutic agents (Swift 2002). One of the straightforward approaches to target amyloid-linked diseases and its associated medical complication is to find potential inhibitors against the onset of amyloid aggregation of proteins. Candidates ranging from single amino acids (Kar and Kishore 2007; Shiraki et al. 2002; Ghosh et al. 2009) and natural products (Stefani and Rigacci 2013) to selected peptides (Etienne et al. 2006; Rajasekhar et al. 2015; Viet et al. 2011) have been reported to interfere with the amyloid aggregation of associated proteins. Few investigations

have also looked at the effect of various nanoparticles on amyloid aggregation of proteins (Alvarez et al. 2013; Majzik et al. 2010; Gao et al. 2011). Citrate-capped gold nanoparticles of size greater than ~20 nm are known to delay the growth rate of α-synuclein aggregation (Alvarez et al. 2013). In a recent study, albumin-modified magnetic nanoparticles were found to promote the depolymerization of insulin amyloid fibrils (Siposova et al. 2012). Successful synthesis of potential gold nanoparticles using various amino acids has been reported recently (Maruyama et al. 2014; Daima et al. 2013). Gold nanoparticles coated with different amino acids have also shown substantial effect on serum albumin absorption and cytotoxicity (Cai et al. 2014).

Therefore, the foundation of the current research was laid on our belief that control of protein aggregation can be efficiently achieved by the presence of amino acid surface corona on the surface of gold and silver nanoparticles, and it may provide additional opportunities to control various physicochemical properties of nanoparticles in controlled manner. For example, amino acids are zwitterionic, and therefore, surface charge of amino acid-coated nanoparticles can be tailored by varying the solution pH. Moreover, the presence of amino acid coating on metal nanoparticles may provide biological identity to nanoparticles.

It is believed that hydrophobic residues including aromatic amino acids play a critical role during amyloid aggregation of proteins (Chiti and Dobson 2009; Fandrich et al. 2001). Since exposed hydrophobic residues are vital to the onset of protein aggregation, adapting a strategy to interfere with the intermolecular hydrophobic interactions may possibly provide an effective approach to inhibit such aggregation process. In accordance with this hypothesis, we have attempted to make metallic nanoparticles surface functionalized with selected hydrophobic residues (tyrosine and tryptophan), and have studied their inhibition effect on amyloid aggregation of a globular protein, insulin.

Here, we demonstrate inhibition of insulin amyloid aggregation using tyrosine-coated gold nanoparticles ($AuNPs^{Tyr}$), tyrosine-coated silver nanoparticles ($AgNPs^{Tyr}$), and tryptophan-coated gold nanoparticles ($AuNPs^{Trp}$). Strong inhibition of both spontaneous and seed-induced aggregation of insulin was observed in the presence of these nanoparticles. We have also carried out bioinformatics analysis and molecular docking studies to understand possible molecular interactions between tyrosine and insulin. Ultimately, this work provides a new approach to target aggregation of proteins by stable nanoparticles coated with aromatic residues.

Materials and methods

Reagents

Tetrachloroauric acid ($HAuCl_4$), $AgNO_3$, L-tryptophan, L-tyrosine, potassium hydroxide (KOH), Thioflavin T, acetic acid, and sodium hydroxide (NaOH) were purchased from Sigma–Aldrich. Deionized MilliQ water was used to prepare various gold and silver nanoparticles. Lyophilized powder of bovine insulin, phosphate buffer saline (PBS), and L-phenylalanine were obtained from HIMEDIA (India).

Synthesis of amino acid-conjugated gold and silver nanoparticles

To synthesize tryptophan and tyrosine amino acid-conjugated gold and silver nanoparticles, 100 ml aqueous solutions of 1 mM KOH containing 0.5 mM tryptophan and 0.1 mM tyrosine were separately allowed to boil under vigorous stirring experimental condition (Selvakannan et al. 2013). In the stirring boiling solutions, $[AuCl_4]^-$ or Ag^+ ions were added to obtain tryptophan or tyrosine amino acid-conjugated gold and silver nanoparticles, respectively. The total concentrations of both the $[AuCl_4]^-$ or Ag^+ metal ions were kept constant at 0.2 mM in all the reactions. Through this process two different gold ($AuNPs^{Tyr}$, $AuNPs^{Trp}$) and silver nanoparticles ($AgNPs^{Tyr}$) solutions were obtained. All these nanoparticle solutions thus obtained were cleaned from the unreduced metal ions and unbound amino acids by dialyzing these solutions against deionized water using 12 kDa dialysis membranes for 3 h followed by overnight dialysis. Even after dialysis, all these gold and silver nanoparticles' solutions remained stable without showing any sign of aggregation, indicating that these nanoparticles were strongly capped with amino acids. All the solutions of tryptophan and tyrosine amino acid-conjugated gold and silver nanoparticles were found to be stable under standard laboratory storage conditions at room temperature for more than 6 months, and used as such for characterization and biological studies.

Fluorescence measurements

A Perkin-Elmer LS 55 fluorescence spectrometer was used to monitor the amyloid aggregation of proteins by Thioflavin T binding assays where Thioflavin T was excited at 440 nm with a slit width of 5 nm and the emission was observed at 490 nm (Morozova-Roche et al. 2000).

UV–Visible spectroscopy

UV–Visible spectrophotometer (Varian Cary-4000 and Shimadzu UV-1800) were used to measure concentrations of protein samples (Dubey et al. 2014) and to obtain UV–Vis spectra of tryptophan-and tyrosine-coated gold and silver nanoparticles.

FTIR spectroscopic analysis

FTIR spectra of tryptophan- and tyrosine-coated gold and silver nanoparticles were recorded in DRS mode using Perkin-Elmer D100 spectrophotometer with a resolution of 4 cm^{-1}.

Amyloid aggregation of insulin

Amyloid aggregation of insulin was studied by incubating the monomer samples (~40 μM) in 10 mM PBS at ~70 °C in the presence and in the absence of $AuNPs^{Tyr}$, $AuNPs^{Trp}$, and $AgNPs^{Tyr}$ nanoparticles (Mark et al. 2004; Chatani et al. 2014). Small aliquots of these aggregating samples were taken out at regular intervals and their Thioflavin T fluorescence intensities were recorded. For conducting seed-induced amyloid aggregation reactions, pre-formed amyloid fibrils (~15 % weight/weight) were used as seeds. For fibril disassembly experiments, a suspension of mature insulin amyloid fibrils was prepared and Thioflavin T signal of the sample was recorded at different time intervals in the presence and absence of $AuNPs^{Tyr}$ (molar ratio of insulin fibrils to $AuNPs^{Tyr}$ was maintained at 1:1).

Circular dichroism spectroscopy

For the CD experiments, JASCO CD spectrometer (model J-815-150 L) with attached Peltier temperature controller was used. The path length of the cell was 2 mm. The structural changes in the protein sample was observed in the presence and absence of $AuNPs^{Tyr}$ and $AuNPs^{Trp}$, by monitoring the CD scans at different time points at 70 °C. Thermal unfolding of insulin was performed by continuously recording the spectra while sample was heated from 25 to 90 °C at a scan rate of 2 °C min^{-1}.

Transmission electron microscopy

Transmission electron microscope (HR-TEM JEOL JEM-2100 and JEOL 1010) was used to examine mature amyloid fibrils and $AuNPs^{Tyr}$, $AuNPs^{Trp}$, and $AgNPs^{Tyr}$ nanoparticles, respectively. Mature amyloid fibril samples were spotted on a carbon-coated grid for 2 min and the samples were then washed with water. The samples were then stained with 1 % (w/v) aqueous uranyl acetate solution for ~2 min followed by another washing step. Air-dried grids were then examined.

Molecular docking and bioinformatics analysis

The structure of ligand (L-tyrosine) was obtained from PubChem (CID 6057) (Bolton et al. 2008) and was prepared using 'prepare ligand wizard' of Discovery studio 4.0 (DS4). X-ray crystal structure of insulin (PDB ID: 4I5Z) (Pechkova et al. 2014) was also prepared through 'prepare protein wizard' of DS4, and pre-processing and protonation were carried out using CHARMm force fields (Brooks et al. 2009). The ligand and protein were then docked using a blind approach (no active site defined) with 100 conformations to choose and 100 orientations to refine by following CDocker protocol (Wu et al. 2003). The complex was then typed with CHARMm force field, and was subjected to molecular dynamics simulation for 5000 picoseconds under NTP (normal temperature and pressure) and distance-dependent dielectrics (implicit solvent model as a crude approximation of polar solvent). The simulations were executed in a Dell precision T5610 workstation with 16 processors and 32 GBs of RAM. Visualizations were performed using DS4. For analysis of crystal structure of bovine insulin multimers, we obtained four multimeric bovine insulin crystal structures from PDB sources (two hetero 12-mers; PDB IDs: 2A3G and 2INS, and two hetero 6-mers; PDB IDs: 2ZP6, 4IDW) (Smith et al. 1982, 2005; Margiolaki et al. 2013). The interface of insulin structures was analyzed to identify the key amino acids involved in multimer formation using DS4. The structures were cleaned by removing water and heteroatoms leaving behind nascent molecules.

Results

Characterization of tyrosine- and tryptophan-coated nanoparticles

Samples of gold nanoparticles coated with tyrosine ($AuNPs^{Tyr}$) and tryptophan ($AuNPs^{Trp}$) and samples of tyrosine-coated silver nanoparticles ($AgNPs^{Tyr}$) were synthesized by following the established protocol (Selvakannan et al. 2013) (see "Synthesis of amino acid-conjugated gold and silver nanoparticles"). SPR absorption bands are considered as characteristic signatures for the existence of stable metal nanoparticles and therefore the formation of nanoparticles can be confirmed using UV–Visible absorption spectroscopy. UV–visible spectra of the obtained nanoparticles are shown in Fig. 1b. $AuNPs^{Tyr}$ and $AgNPs^{Tyr}$ nanoparticles showed typical SPR bands at ~523 and ~417 nm, respectively, wherein the SPR absorbance peak

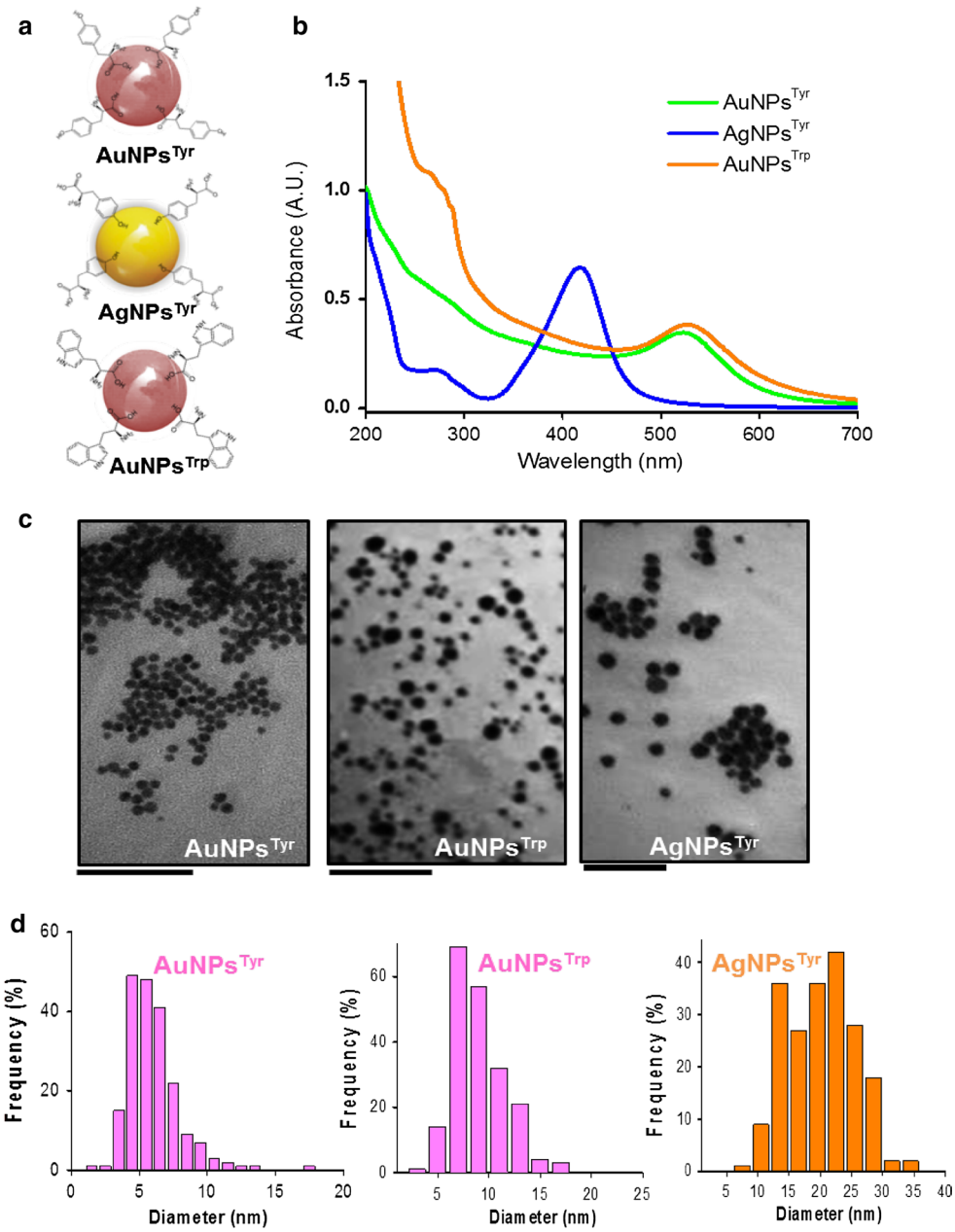

Fig. 1 Characteristic features of tyrosine- and tryptophan-coated nanoparticles. **a** Schematic representation of tyrosine ($AuNPs^{Tyr}$ and $AgNPs^{Tyr}$)- and tryptophan ($AuNPs^{Trp}$)-coated nanoparticles. The orientation of the attachment of tyrosine residues is reversed in the silver nanoparticles ($AgNPs^{Tyr}$). **b** UV–Visible spectra of the nanoparticle samples: (*olive curve*) $AuNPs^{Tyr}$; (*orange curve*) $AuNPs^{Trp}$; and (*violet curve*) $AgNPs^{Tyr}$. **c** Transmission electron microscopic images of $AuNPs^{Tyr}$, $AuNPs^{Trp}$, and $AgNPs^{Tyr}$. The *scale bar* represents 100 nm. The average diameter of the nanoparticles was observed to fall within ~15–30 nm. **d** Particles size histograms corresponding to tyrosine- and tryptophan-coated $AuNPs^{Tyr}$, $AuNPs^{Trp}$, and $AgNPs^{Tyr}$ nanoparticles. This analysis was done by using ImageJ software (color figure online)

of $AuNPs^{Trp}$ sample was observed at ~525 nm. The SPR absorption curves of $AuNPs^{Tyr}$, $AuNPs^{Trp}$, and $AgNPs^{Tyr}$ nanoparticles look very similar to the reported values for similar nanoparticles. Transmission electron micrographs of $AuNPs^{Tyr}$, $AuNPs^{Trp}$, and $AgNPs^{Tyr}$ samples are shown in Fig. 1c. All these nanoparticles appeared spherical displaying a uniform diameter value of ~10–30 nm by analysis of TEM images using ImageJ tools. These amino acid-capped nanoparticles were also observed to be very stable and we did not see any sign of aggregation even after 6 months of storage time.

FTIR spectroscopic analysis of gold and silver nanoparticles synthesized by tryptophan and tyrosine was carried out to understand the surface chemistry of different nanoparticles and to provide direct evidence of amino acids interaction with the nanoparticles. FTIR data are presented in supplementary Figure S14 which shows vibrational frequencies in tryptophan- and tyrosine-coated nanoparticles. The shift of the carbonyl stretching frequency of tryptophan from *1666 cm^{-1} (magenta curve, Figure S14) to 1707 cm^{-1} was observed for $AuNPs^{Trp}$ (blue curve, Figure S14). Tyrosine has a carbonyl stretching frequency around *1610 cm^{-1} (green curve, Figure S14) that shifted to 1740 cm^{-1} in case of $AuNPs^{Tyr}$ and $AgNPs^{Tyr}$ (red and black curves Figure S14) after the synthesis of nanoparticles.

Inhibition of insulin amyloid aggregation

Amyloid aggregation of insulin in PBS was studied at an elevated temperature, ~70 °C (close to the T_m of insulin) by monitoring the rise in the Thioflavin T signal at different time points (see "Materials and methods"). Soluble insulin monomers at ~40 μM showed a characteristic aggregation curve (Fig. 2, *filled circle*) composing of a distinct lag phase, a growth phase, and a saturation phase. Final aggregates of insulin showed typical amyloid morphology (Fig. 3c) as seen in the previous studies (Mark et al. 2004). The inhibition effect of amino acid-coated nanoparticles was examined at three different molar ratio values (of insulin:inhibitor) as mentioned in Fig. 2. Both AuNPs^{Tyr} and AuNPs^{Trp} showed dose-dependent inhibition of insulin amyloid aggregation (Fig. 2a, b). Control experiments of insulin aggregation in the presence of the solvents and solutes used for nanoparticle preparation did not show any inhibition effect (data not shown).

To confirm the inhibition effect of coated tyrosine and tryptophan residues, as a next step, we tested the effect of isolated aromatic residues (phenylalanine, tyrosine, and tryptophan) on amyloid aggregation of insulin. The data as shown in Fig. 2d clearly indicate that the control insulin sample and the amino acid-treated sample follow similar kinetics during amyloid aggregation. This result confirms that tyrosine and tryptophan molecules are effective in inhibiting the amyloid aggregation only when they are attached to the surface of the nanoparticles. The inhibition effect of AuNPs^{Tyr} was found to be slightly more suppressing than the effect observed for AuNPs^{Trp} at similar concentration (Fig. 2a, *filled triangle*, b, *inverted filled triangle*).

Next, we performed experiments to know the effect of these nanoparticles on seed-induced aggregation of insulin.

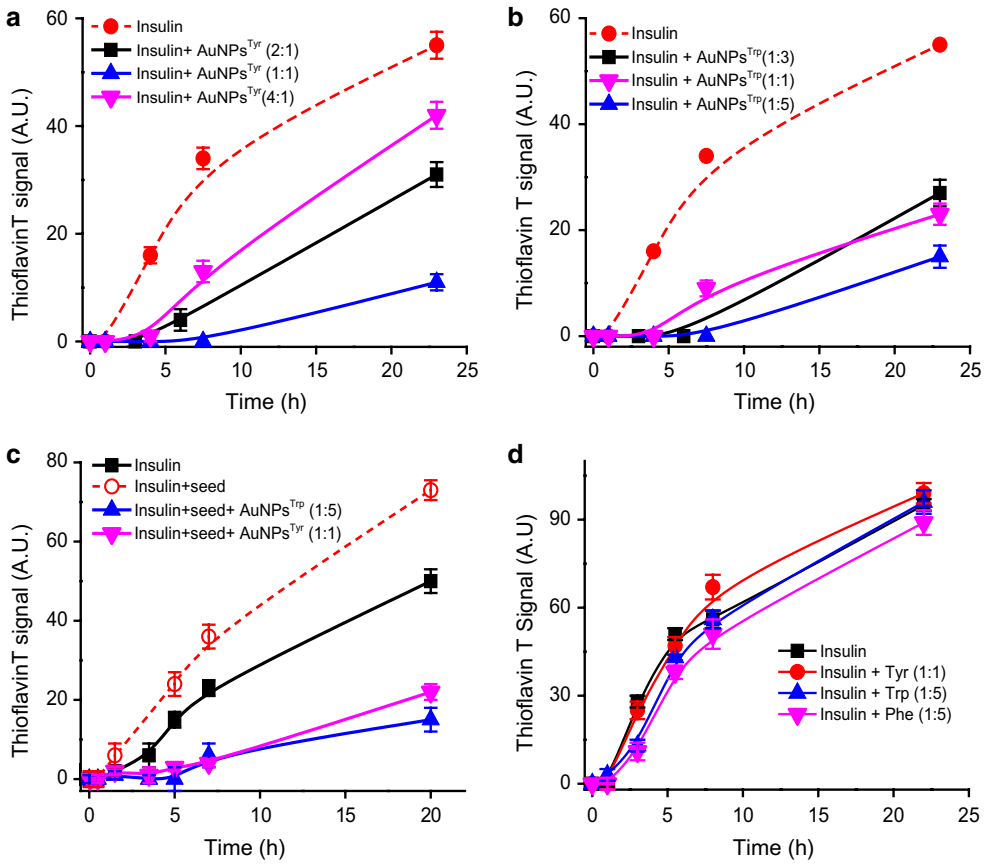

Fig. 2 Inhibition of insulin amyloid aggregation by tyrosine- and tryptophan-coated nanoparticles. **a** Effect of AuNPs^{Tyr} on aggregation of ~40 μM insulin sample at different values of molar ratio: (*filled circle*) insulin; (*inverted filled triangle*) insulin + AuNPs^{Tyr} at 4:1; (*filled square*) insulin + AuNPs^{Tyr} at 2:1; (*filled triangle*) insulin + AuNPs^{Tyr} at 1:1. **b** Effect of AuNPs^{Trp} on spontaneous aggregation of ~40 μM insulin at different molar ratios: (*filled circle*) insulin only; (*inverted filled triangle*) insulin + AuNPs^{Trp} at 1:1 molar ratio; (*filled square*) insulin + AuNPs^{Trp} at 1:3 molar ratio; (*filled triangle*) insulin + AuNPs^{Tyr} at 1:5 molar ratio. **c** Effect of AuNPs^{Tyr} and AuNPs^{Trp} on seed-induced aggregation of insulin (*filled square*) insulin only; (*open circle*) insulin + 15 % (w/w) seed; (*inverted filled triangle*) insulin + seed + AuNPs^{Tyr} at 1:1 molar ratio; (*filled triangle*) insulin + seed + AuNPs^{Trp} at 1:5 molar ratio. **d** Effect of isolated tyrosine, tryptophan and phenylalanine residues on aggregation of insulin: (*filled square*) insulin only; (*filled circle*) insulin + Tyr at 1:1; (*filled triangle*) insulin + Trp at 1:5; (*inverted filled triangle*) insulin + Phe at 1:5 molar ratio (color figure online)

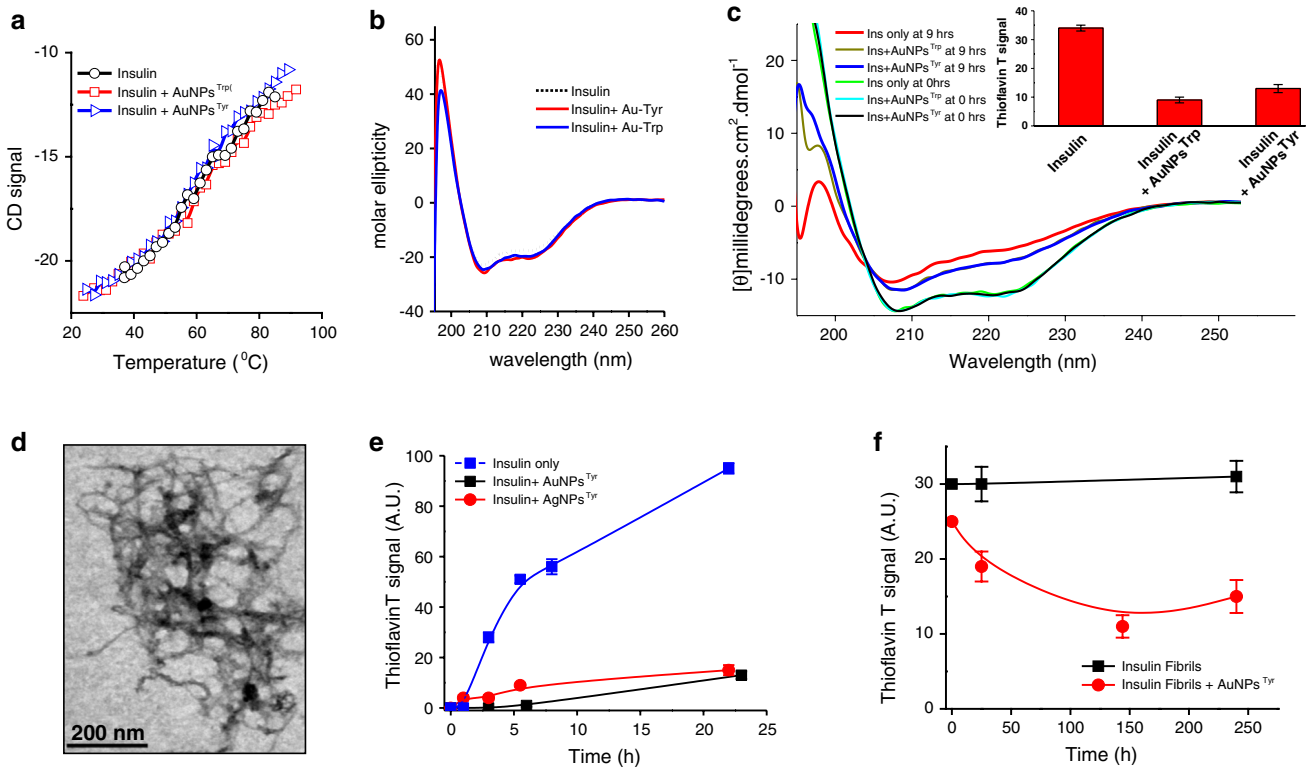

Fig. 3 **a** CD spectra of insulin in the presence and absence of Trp- and Tyr-coated nano particles: (*dotted curve*) insulin only; (*red curve*) insulin + AuNPs^{Tyr} at 1:1 molar ratio; (*violet curve*) insulin + AuNPs^{Trp} at 1:5 molar ratio. **b** Thermal unfolding of insulin by circular dichroism by monitoring change of CD signal at ~222 nm: (*open circle*) insulin only; (*open square*) insulin + AuNPs^{Tyr} at 1:1 ratio; (*right headed open triangle*) insulin + AuNPs^{Trp} at 1:5 molar ratio. **c** CD spectra of insulin undergoing aggregation in the presence and absence of nanoparticles: insulin only at 0 h; (*olive curve*) and 9 h (*red curve*); insulin + AuNPs^{Tyr} at 1:1 molar ratio at 0 h (*black curve*) and at 9 h (*violet curve*); insulin + AuNPs^{Trp} at 1:1 molar ratio at 0 h (*blue curve*) and at 9 h (*black curve*). *Inset* shows ThT signal of the CD samples at 9 h. **d** TEM image of insulin mature amyloid fibrils. **e** Comparison of the effect of AuNPs^{Tyr} and AgNPs^{Tyr} on spontaneous aggregation of ~43 μM insulin: (*filled square*) insulin only; (*filled circle*) insulin + AgNPs^{Tyr} at 1:1 molar ratio; (*filled square*) insulin + AuNPs^{Tyr} at 1:1 molar ratio. **f** Effect of tyrosine-coated nanoparticles on disassembly of mature amyloid fibrils of insulin: (*filled square*) insulin fibrils; (*filled circle*) insulin fibrils + AuNPs^{Tyr} at 1:1 molar ratio of insulin:tyrosine (color figure online)

In the presence of seed (~15 % w/w), we observed a rapid rise in the Thioflavin T signal without a lag phase. However, inhibition of seed-induced aggregation was observed in the presence of AuNPs^{Tyr} (Fig. 2c, *inverted filled triangle*) and AuNPs^{Trp} (Fig. 2c, *filled triangle*) nanoparticles. It appears that these nanoparticles have the ability to interfere with the recruitment of the monomers by mature fibrils which in turn suppresses the seeded elongation during aggregation process. To further clarify the interaction between the AuNPs^{Tyr} and mature fibrils, we examined whether the nanoparticles have the ability to promote dissociation of amyloid fibrils. To conduct disassembly experiments, AuNPs^{Tyr} sample was added to a suspension of mature insulin fibrils, and Thioflavin T signal of the sample was monitored at different time intervals. The obtained data as shown in Fig. 3f clearly indicate that AuNPs^{Tyr} promote disassembly of insulin amyloid fibrils. After ~240 h of incubation, we observed almost ~50 % decrease of the initial Thioflavin T signal (Fig. 3f, *filled cirlce*) which suggests a substantial amount of fibril dissociation in the presence of AuNPs^{Tyr}. In a previous study, it was reported that albumin modified magnetic fluid causes the depolymerization of insulin amyloid fibrils (Siposova et al. 2012).

Effect on conformational properties of insulin

Since both AuNPs^{Tyr} and AuNPs^{Trp} showed their potential either to inhibit or to interfere with amyloid aggregation of insulin, we used circular dichroism (CD) measurements to understand whether these nanoparticles have any effect on the conformational properties of insulin. First, we examined the CD spectra of the insulin sample in the presence and absence of nanoparticles. The molecular conformation of insulin remained unchanged in the presence of nanoparticles (Fig. 3b). Next, we performed thermal unfolding of insulin in PBS by monitoring the change in the CD signal at ~222 nm. The thermal unfolding curves showed no significant change in the T_m values of insulin samples in the

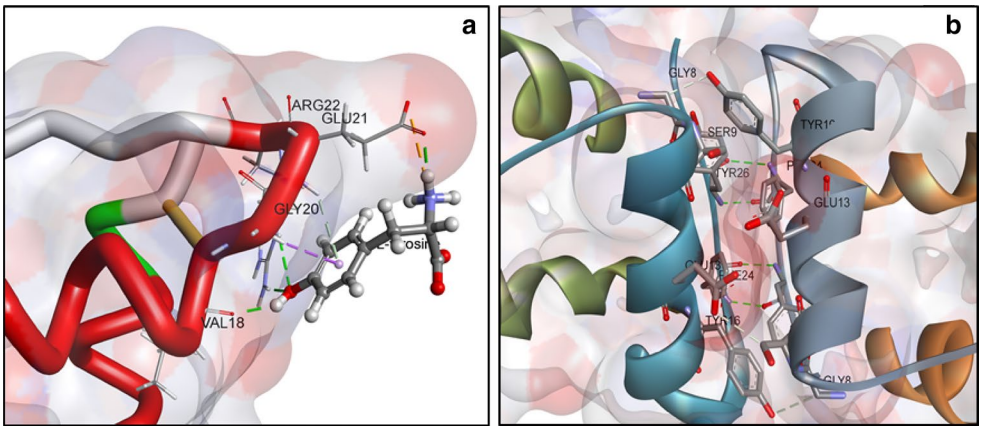

Fig. 4 **a** Molecular docking studies of a tyrosine molecule with insulin. The complex shows seven interactions comprising of four hydrogen bonds (B:ARG22:HE—L-tyrosine:O14, B:ARG22:HH21—L-tyrosine:O14, B:GLU21:OE1—L-tyrosine:H21, and B:VAL18:O—L-tyrosine:H24), two pi interactions (B:GLU21:HN—L-tyrosine, B:GLY20:HA1—L-tyrosine), and one electrostatic bond (B:GLU21:OE2—L-tyrosine:N13). **b** Analysis of a crystal structure of insulin dimer to visualize the binding partners of tyrosine residue of one insulin molecule with different functional groups of another insulin molecule at the interface region. Discovery Studio 4.0 was used for the docking studies

presence of these nanoparticles (Fig. 3a, *open square*, *open circle,* and *right-headed open triangle*).

To understand the structural changes during inhibition of aggregation, we also monitored the CD signal of aggregating insulin samples in the presence of and absence of both $AuNPs^{Tyr}$ and $AuNPs^{Trp}$. Figure 3c compares the CD spectra of both inhibited and uninhibited reactions measured at 0 and 9 h. Data clearly indicate that the process of conversion of native insulin molecules into β-structured species is delayed in the presence of nanoparticles (Fig. 3c, blue curve and olive curve). Thioflavin T readings of the same samples are almost consistent with the observed CD data (inset of Fig. 3c).

Molecular docking of tyrosine with insulin

To further understand the observed inhibition effect, we carried out molecular docking studies on insulin-tyrosine interactions. Blind docking studies (see "Materials and methods") predicted a viable tyrosine–insulin interaction at a site within insulin's B-chain which spans from Val18–Arg22. The value of CDocker energy for the best pose (as shown in Fig. 4a) was -29.02 kcal mol^{-1} and its corresponding interaction energy was observed to be -22.95 kcal mol^{-1}. Such energy values suggest the formation of a stable protein–ligand complex. Obtained tyrosine–insulin complex as shown in Fig. 4a displays seven interactions composing of four hydrogen bonds (B:ARG22:HE—L-tyrosine:O14, B:ARG22:HH21—L-tyrosine:O14, B:GLU21:OE1—L-tyrosine:H21, and B:VAL18:O—L-tyrosine:H24), two pi interactions (B:GLU21:HN—L-tyrosine, B:GLY20:HA1—L-tyrosine), and one electrostatic bond (B:GLU21:OE2—L-tyrosine:N13). The stability of insulin–tyrosine complex was further ascertained using molecular dynamics study. Both root-mean square deviation and total energy of the complex indicated the formation of a stable conformation after 5000 ps (Figure S4, supplementary information). These data suggest that tyrosine's docking site spans from Val18–Arg22 region of insulin's chain B and binding of tyrosine to that region of insulin may perhaps result in a stable protein–ligand complex. We further carried out the docking studies on insulin–alanine and insulin–tryptophan interactions. The obtained data (Figure S10, S11, S12, and S13 in the supplementary information) suggest that the number of hydrogen bonds formed between ligand and the protein is highest when the ligand is tyrosine and is lowest when the ligand is alanine. Further the molecular dynamics studies of tyrosine–insulin complex formation predicts a more favorable complex in terms of energy and RMSD than that of insulin-alanine and insulin-tryptophan interactions (Figure S12).

To further clarify the possible binding partners of a tyrosine residue when it interacts with insulin, we looked at the available crystal structures of insulin dimers (PDB IDs: 2A3G, 2INS, 2ZP6, and 4IDW) (Smith et al. 1982, 2005; Margiolaki et al. 2013). We focused on the interface of insulin–insulin dimers and analyzed the involvement of tyrosine residues in intermolecular interactions. Tyr16–Tyr26 region of chain B of insulin was found to be mediating important H-bonding interactions with average hydrogen bond length of 3.055 Å. Further data analysis (Figure S5–S8, supplementary information) clearly indicates that tyrosine residues are playing a key role during insulin–insulin dimer formation (Figure S8, S9, supplementary information).

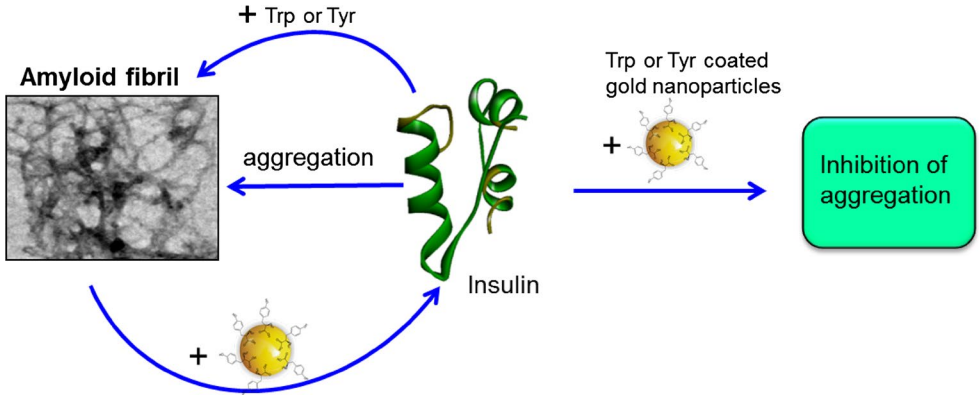

Fig. 5 Schematic representation of inhibition of insulin amyloid formation and promotion of amyloid dissociation in the presence of Tyrosine- and Tryptophan-coated gold nanoparticles

Effect of reversing the orientation of tyrosine attached to nanoparticles

Because the bioinformatics analysis and tyrosine–insulin docking studies indicate involvement of tyrosine's aromatic moiety, C=O and $–NH_2$ functional groups, the question of whether the orientation of the attached tyrosine molecule is vital to its inhibition effect is very significant. To clarify which functional groups are important for the observed inhibition effect, we strategically (Selvakannan et al. 2013) synthesized $AgNPs^{Tyr}$ sample, where the orientation of the attached tyrosine molecules is reversed (Fig. 1a, c and Figure S2 of supplementary information). The reverse orientation of oxidized tyrosine has been confirmed in our previous study by XPS and zeta potential measurements, wherein the amine group of tyrosine molecule binds with gold nanoparticle surface and the semiquinone group of tyrosine binds with the silver nanoparticle surface (Selvakannan et al. 2013). Hence unlike the gold nanoparticles ($AuNPs^{Tyr}$), the $–NH_2$ and C=O groups of the tyrosine molecules in $AgNPs^{Tyr}$ would be protruding outward facing the solvent. Inhibition of amyloid aggregation of insulin was also observed in the presence of such $AgNPs^{Tyr}$ nanoparticles. However, the inhibition effect of $AgNPs^{Tyr}$ was found to be slightly lesser than the observed inhibition effect for $AuNPs^{Tyr}$ (Fig. 3d). This data is consistent with the results obtained from insulin–tyrosine docking studies which also suggest the occurrence of interactions mediated through C=O and $–NH_2$ groups of tyrosine.

Discussion

Current study clearly reveals the potential of the nanoparticles coated with aromatic residues to inhibit amyloid aggregation of insulin. A schematic representation of the current results is given in Fig. 5. Because such inhibition effect is not observed in the presence of isolated tyrosine and tryptophan residues, it is predicted that surface functionalization of these aromatic residues is critical for their anti-amyloid efficacies. Such functionalization would preferably allow the functional groups of the ligand molecules to participate in crucial interactions with the corresponding functional groups of the protein molecule at the site of binding. Our computational studies predict tyrosine's ability to participate in H-bond, CH-π bond, and electrostatic interactions (Fig. 4a, b). The contribution of the aromatic moiety of tyrosine seems to be larger than the participation mediated through the C=O and $–NH_2$ groups of tyrosine. This could be one of the reasons behind the slight reduction in the inhibition ability of tyrosine when the molecule's orientation was reversed during surface functionalization (attachment with the nanoparticles through its phenolic –OH group) (Fig. 3e, $AgNPs^{Tyr}$).

Inhibition of both seed-induced aggregation and spontaneous aggregation reveals two vital clues: (1) These nanoparticles may perhaps bind to insulin monomers undergoing aggregation; (2) They might well bind to the available growing ends of the mature amyloid fibrils blocking the recruitment of monomers. It is also possible that these nanoparticles have the potential to interact with both the monomeric and the fibrillar forms of insulin. This hypothesis is further supported by promotion of the fibril disassembly by AuNPs. Chain B of insulin is known to be the amyloid-prone region of insulin (Tartaglia et al. 2008). Studies have shown that the isolated chain B peptide of bovine insulin also forms amyloid fibrils (Hong and Fink 2005). The site of tyrosine binding, as predicted by our docking studies, falls within the chain B of insulin. Further, the analysis of crystal structures of insulin dimers clearly shows significant contribution by tyrosine residues, particularly at the interface site, connecting two insulin molecules (Fig. 4b, supplemental Information figure S4–S9). Occurrence of such interactions directly supports the possibility of binding of the surface functionalized tyrosine molecules (of the nanoparticles) to insulin by interacting with residues of its chain B and such interactions may interfere with the self-assembly process of insulin monomers into amyloid fibrils. This assumption is further supported by monitoring the change in the conformation of

insulin in an inhibited aggregation reaction which shows the retention of insulin's native conformation (Fig. 3d). However, the T_m of insulin in the presence of $AuNPs^{Tyr}$ and $AuNPs^{Trp}$ remained unchanged (Fig. 3a). It is possible that the nanoparticle–insulin interaction may influence the equilibrium of the [Intermediate ⇋ Aggregate] reaction to shift to the left without enhancing the thermal stability of intermediate species of insulin. This is further supported by the evidence of promotion of insulin fibril dissociation in the presence of tyrosine-coated gold nanoparticles. Aromatic residues are not only important to amyloid aggregation of proteins but they are also known to play critical roles during protein–protein interactions (Bhattacharyya and Chakrabarti 2003). The driving force for amyloid aggregation is believed to arise from favorable interactions between partially folded intermediate species. In the case of globular proteins, such intermediate species are predicted to expose their buried hydrophobic residues to the solvent. Here, the strategy to target intermolecular hydrophobic interaction by nanoparticles coated with aromatic residues is certainly unique and such approach may possibly offer a broader utility of its applications.

In summary, we have identified three important properties of tyrosine- and tryptophan-coated nanoparticles: (a) strong inhibition of spontaneous aggregation of insulin; (b) suppression of seed-induced aggregation of insulin; and (c) promotion of disassembly of insulin amyloid aggregates. Although these results are observed in an in vitro system, it is possible that such inhibition properties may be seen in other amyloid systems including in vivo studies. With such multiple efficacies, these nanoparticles may offer an attractive approach for both production and formulation of effective anti-amyloid candidates.

Acknowledgments We thank IIT Jodhpur for research facilities. We thank IIT Bombay for use of the Cryo HR-TEM Central Facility. This work was supported by BRNS grant (KK) (Grant No.37(1)/14/38/2014-BRNS) and Seed Grant from Indian Institute of Technology Jodhpur (KK and GB). HKD gratefully acknowledges Department of Science and Technology (DST), Government of India for ITS Grant (Grant No. SB/ITS-Y/0988/2014-15).

Compliance with ethical standards

Conflict of interest The authors declare that they have no conflict of interest.

References

Aguzzi A, O'Connor T (2010) Protein aggregation diseases: pathogenicity and therapeutic perspectives. Nat Rev Drug Discovery 9:237–248

Alvarez YD, Fauerbach JA, Pellegrotti JV, Jovin TM, Jares-Erijman EA, Stefani FD (2013) Influence of gold nanoparticles on the kinetics of α-synuclein aggregation. Nano Lett 13:6156–6163

Bhattacharyya R, Chakrabarti P (2003) Stereospecific interactions of proline residues in protein structures and complexes. J Mol Biol 331:925–940

Bolton EE, Wang Y, Thiessen PA, Bryant SH (2008) PubChem: integrated platform of small molecules and biological activities. Ann Rep Comput Chem 4:217–241

Brooks BR, Brooks CL III, Mackerell AD Jr, Nilsson L, Petrella RJ, Roux B, Won Y, Archontis G, Bartels C, Boresch S et al (2009) CHARMM: the biomolecular simulation program. J Comput Chem 30:1545–1614

Cai H, Yao P (2014) Gold nanoparticles with different amino acid surfaces: serum albumin adsorption, intracellular uptake and cytotoxicity. Colloids Surf B Biointerfaces 123:900–906

Chatani E, Imamura H, Yamamoto N, Kato M (2014) Stepwise organization of the β-structure identifies key regions essential for the propagation and cytotoxicity of insulin amyloid fibrils. J Biol Chem 289:10399–10410

Chiti F, Dobson CM (2006) Protein misfolding, functional amyloid, and human disease. Ann Rev Biochem 75:333–366

Chiti F, Dobson CM (2009) Amyloid formation by globular proteins under native conditions. Nat Chem Biol 5:15–22

Daima HK, Selvakannan PR, Shukla R, Bhargava SK, Bansal V (2013) Fine-tuning the antimicrobial profile of biocompatible gold nanoparticles by sequential surface functionalization using polyoxometalates and lysine. PLoS ONE 8:e79676

Dubey K, Anand BG, Temgire MK, Kar K (2014) Evidence of rapid coaggregation of globular proteins during amyloid formation. Biochemistry 53:8001–8004

Etienne MA, Aucoin JP, Fu Y, McCarley RL, Hammer RP (2006) Stoichiometric inhibition of amyloid beta-protein aggregation with peptides containing alternating alpha, alpha-disubstituted amino acids. J Am Chem Soc 128:3522–3523

Fandrich M, Fletcher MA, Dobson CM (2001) Amyloid fibrils from muscle myoglobin. Nature 410:165–166

Gao N, Zhang Q, Mu Q, Bai Y, Li L, Zhou H, Butch ER, Powell TB, Snyder SE, Jiang G, Yan B (2011) Steering carbon nanotubes to scavenger receptor recognition by nanotube surface chemistry modification partially alleviates NFkappaB activation and reduces its immunotoxicity. ACS Nano 5:4581–4591

Ghosh R, Sharma S, Chattopadhyay K (2009) Effect of arginine on protein aggregation studied by fluorescence correlation spectroscopy and other biophysical methods. Biochemistry 48:1135–1143

Greenwald J, Riek R (2010) Biology of amyloid: structure, function, and regulation. Structure 18:1244–1260

Hong DP, Fink AL (2005) Independent heterologous fibrillation of insulin and its B-chain peptide. Biochemistry 44:16701–16709

Kar K, Kishore N (2007) Enhancement of thermal stability and inhibition of protein aggregation by osmolytic effect of hydroxyproline. Biopolymers 87:339–351

Majzik A, Fulop L, Csapo E, Bogar F, Martinek T, Penke B, Biro G, Dekany I (2010) Functionalization of gold nanoparticles with amino acid, beta-amyloid peptides and fragment. Colloids Surf B Biointerfaces 81:235–241

Margiolaki I, Giannopoulou AE, Wright JP, Knight L, Norrman M, Schluckebier G, Fitch AN, Von Dreele RB (2013) High-resolution powder X-ray data reveal the T(6) hexameric form of bovine insulin. Acta Crystallogr D Biol Crystallogr 69:978–990

Mark RH, Krebs LA, Morozova-Roche KD, Carol VR, Dobson CM (2004) Observation of sequence specificity in the seeding of protein amyloid fibrils. Protein Sci 13:1933–1938

Maruyama T, Fujimoto Y, Maekawa T (2014) Synthesis of gold nanoparticles using various amino acids. J Colloid Interface Sci. doi:10.1016/j.jcis.2014.12.046

Morozova-Roche LA, Zurdo J, Spencer A, Noppe W, Receveur V, Archer DB, Joniau M, Dobson CM (2000) Amyloid fibril

formation and seeding by wild-type human lysozyme and its disease-related mutational variants. J Struct Biol 130:339–351

Pechkova E, Bragazzi N, Bozdaganyan M, Belmonte L, Nicolini C (2014) A review of the strategies for obtaining high-quality crystals utilizing nanotechnologies and microgravity. Crit Rev Eukaryot Gene Expr 24:325–339

Rajasekhar K, Suresh SN, Manjithaya R, Govindaraju T (2015) Rationally designed peptidomimetic modulators of abeta toxicity in Alzheimer's disease. Sci Rep 5:8139

Selvakannan P, Ramanathan R, Plowman BJ, Sabri YM, Daima HK, O'Mullane AP, Bansal V, Bhargava SK (2013) Probing the effect of charge transfer enhancement in off resonance mode SERS via conjugation of the probe dye between silver nanoparticles and metal substrates. Phys Chem Chem Phys 15:12920–12929

Shiraki K, Kudou M, Fujiwara S, Imanaka T, Takagi M (2002) Biophysical effect of amino acids on the prevention of protein aggregation. J Biochem 132:591–595

Siposova K, Kubovcikova M, Bednarikova Z, Koneracka M, Zavisova V, Antosova A, Kopcansky P, Daxnerova Z, Gazova Z (2012) Depolymerization of insulin amyloid fibrils by albumin-modified magnetic fluid. Nanotechnology 23:055101

Smith GD, Duax WL, Dodson EJ, Dodson GG, de Graaf RAG, Reynolds CD (1982) The structure of Des-Phe B1 bovine insulin. Acta Crystallogr Sect B Struct Crystallogr Cryst Chem 38:3028–3032

Smith GD, Pangborn WA, Blessing RH (2005) The structure of T6 bovine insulin. Acta Crystallogr D Biol Crystallogr 61:1476–1482

Stefani M, Rigacci S (2013) Protein folding and aggregation into amyloid: the interference by natural phenolic compounds. Int J Mol Sci 14:12411–12457

Swift B (2002) Examination of insulin injection sites: an unexpected finding of localized amyloidosis. Diabet Med J Br Diabet Assoc 19:881–882

Tartaglia GG, Pawar AP, Campioni S, Dobson CM, Chiti F, Vendruscolo M (2008) Prediction of aggregation-prone regions in structured protein. J Mol Biol 380:425–436

Viet MH, Ngo ST, Lam NS, Li MS (2011) Inhibition of aggregation of amyloid peptides by beta-sheet breaker peptides and their binding affinity. J Phys Chem B 115:7433–7446

Wu G, Robertson DH, Brooks CL, Vieth M (2003) Detailed analysis of grid-based molecular docking: a case study of CDOCKER-A CHARMm-based MD docking algorithm. J Comput Chem 24:1549–1562